Feasibility of X-ray scattering for tracer-free liquid-phase thermometry for multiphase flows

B. R. HALLS,[1*] N. RAHMAN,[2] K. E. MATUSIK,[3] T. R. MEYER,[2] AND A. L. KASTENGREN[4]

[1]Sandia National Laboratories, Engineering Sciences Center, Albuquerque, NM 87185

[2]School of Mechanical Engineering, Purdue University, West Lafayette, IN 47907

[3]Sigray, Concord, CA 94520

[4]X-Ray Science Division, Argonne National Laboratory, Lemont, IL 60439

*brhalls@sandia.gov

Abstract: The feasibility of liquid temperature measurements using X-ray scattering is investigated for liquids with varying properties (water, ethanol, and *n*-dodecane) on beamline 7-BM at the Advanced Photon Source at Argonne National Laboratory. The temperature is inferred through the change in the scattering pattern from the liquid as a function of temperature using partial least squares regression. An accuracy of ~98% or higher was achieved enabling measurements for a wide range of applications.

Introduction

A major challenge faced by the transportation and power generation industries is the safe and reliable delivery of fuel, both *en route* to the engine and/or within the combustor [1]. *In situ* measurement of the liquid temperature is important for understanding fuel icing and thermal stability, which are important considerations for aviation engine operation at extreme conditions. The fuel temperature during injection is key to understanding mixing and vaporization of complex

and alternative fuels due to its impact on surface coking, pollutant emissions, combustion instabilities, overall efficiency, and component reliability [2–4].

The current state-of-the-art optical techniques for *in situ* measurement of the temperature of droplets and sprays during fuel injection has been reviewed by Lemoine and Castanet [5], and include: elastic scattering methods [6,7], laser-induced fluorescence (LIF) and laser-induced exciplex fluorescence (LIEF) [8–12], laser-induced phosphorescence [13,14], thermographic phosphors [15], inelastic Raman scattering [16] and infrared thermometry [17].

The use of X-rays is an alternative to these optical techniques, which are susceptible to refraction and multiple scattering events in optically dense sprays and may require tracers. Because X-ray attenuation via photoelectric absorption and molecular scattering dominate over interfacial scattering in the X-ray area of interest (5–100 keV), accurate measurements of liquid mass distribution can be made even in the presence of complex liquid structures. Such measurements have been developed using both laboratory scale tube sources [21,22] and synchrotron sources [23–28]. Various measurement modalities have been explored including radiography [21–24], computed tomography [22], X-ray fluorescence [23,25], phase contrast imaging [23,26], and small angle scattering [27].

Recently, X-ray elastic scattering and diffraction have also been used to measure the short-range order and molecular spacing in a supercooled water droplet stream [33]. Ice crystals demonstrate powder diffraction patterns due to the long-range order in the ice crystals. However, liquid water lacks this long-range order. Instead, liquid water demonstrates a diffuse ring of scattering at a scattering vector magnitude of $q = 1.5–3.5$ $Å^{-1}$. As the scattering pattern depends on the intermolecular spacing between water molecules and, hence, temperature, it is of interest to determine the feasibility of utilizing this phenomenon for thermometry in liquid fuels. The use of

X-rays enables the application of this approach in chaotic multiphase flows (intact liquid or droplet fields) where high levels of attenuation and multiple scattering events can inhibit visible light diagnostics, particularly in the spray formation region. The expected SNR is a function of the liquid mass within the probe volume and the integration time. Therefore, this approach is well suited for optically complex and/or dense sprays rather than in dilute regions where the spray is more broadly dispersed. As the X-ray scatting patterns are unique to the fluid present and no tracers or dopants are required, the signals could also be used to isolate certain liquids from surrounding gases and coflows.

Experimental Setup

The X-ray scattering measurements were conducted in the 7-BM beamline at the Advanced Photon Source (APS) at Argonne National Laboratory. The 7-BM white beam was filtered with a double multilayer monochromator (1.2% $\Delta E/E$) at 15 keV mean photon energy. This beam was focused with a pair of Kirkpatrick-Baez focusing mirrors to a 5×6 μm^2 full width at half maximum (FWHM) focus, with a convergence angle of less than 3 mrad [34]. More information on the 7-BM beamline can be found in Kastengren and Powell, 2014 [28].

Figure 1 shows a schematic of the experimental concept, which relies on the interference pattern generated by elastic scattering from the electrons in the atomic shell. The pattern depends on the spacing of the molecules, which is influenced by temperature. To test this concept, the 15 keV X-ray beam intersected the center of a 0.5 mm diameter liquid jet at a known temperature placed at the incident beam focus. The transmitted X-ray beam was collected with a 300 μm thick Si PIN diode and transimpedance amplifier. The scattered X-rays were collected with a photon counting pixel array detector (Dectris, Pilatus 100K, 487 x 195 pixels, 172 x 172 μm^2 pixel size) placed downstream and offset from the transmitted beam. Shielding and guard slits were used to minimize

illumination of the pixel array detector by the scattering from beamline optics and air. The liquid jet was translated through the beam to map out the mass distribution (using NIST coefficients [35]) and temperature via radiography and scattering, respectively. The spatial resolution along the scanned horizontal axis was determined by the scan spacing of 50 μm. The scattering signal was averaged for 10 seconds at each temperature and the image on the detector was binned on lines of constant scattering angle. The noise in the scattering pattern (measured at the peak intensity) was approximately 4%, which after filtering was reduced to less than 0.1% and did not play a significant role in the analysis.

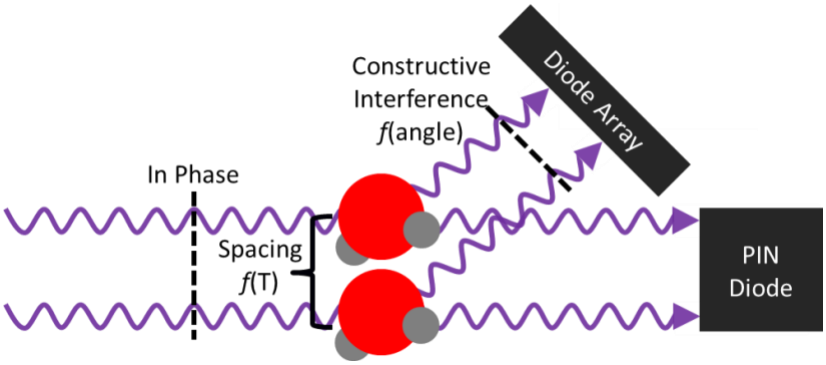

Fig. 1. Experimental concept of the interaction between the X-rays and liquid molecules. The out-of-phase scattered photons form interference patterns on the diode array detector as a function of the molecular spacing and scattering angle. Transmitted photons are collected by a PIN diode to measure the equivalent path length of liquid.

This approach was applied to water, a common surrogate in spray measurements and a component in fuel icing studies; ethanol, which is a common alcohol solvent and fuel additive; and *n*-dodecane, a high molecular weight alkane fuel component in transportation, power generation, and industrial processing. The temperature of the liquids prior to injection was controlled via a water bath with heat exchanger (limiting the lower range of temperatures to just above that of freezing water) and monitored with a thermocouple mounted close to the injection nozzle. Each liquid was

measured at approximately 100 temperature increments over various ranges, including water from 276 to 360 K (2.5–87 °C), ethanol from 279 K to 338 K (5.9–65 °C), and *n*-dodecane from 280 K to 341 K (7–68 °C). The liquid was injected into air at room temperature and ambient pressure at relatively low upstream pressure such that little atomization or droplet breakup occurred in the liquid jets. The largest estimated temperature drop of the liquid from the thermocouple to the measurement region was less than 1 K, and the estimated temperature increase from the X-ray beam was estimated to be less than 0.01 K, based on the liquid flow rate, beam size, and X-ray absorption in the liquid.

The X-ray scattering pattern is properly given as a function of the scattering vector magnitude q, defined as: $q = 4\pi/\lambda \sin(\theta/2)$, where λ is the X-ray wavelength and θ is the full scattering angle. Powder diffraction imaging of lanthanum hexaboride (LaB_6) as a reference material with a known powder diffraction pattern was used to calibrate the detector, as shown in Fig 2(a). The rings are compared against reference values after azimuthal integration, as seen in Fig. 2(b), with <0.3% error in the fits of each peak. Figure 2(c) shows the scattering intensity distribution collected by the detector of liquid water at 4 K, along with the azimuthal integration of this image in Fig. 2(d) showing line plots in its raw form (after background subtraction) and filtered form. A Savitzky-Golay 3rd order filter of window length 49 pixels was also applied to each of the scattering patterns to reduce the noise in Fig 2(d). The background scattering (no liquid jet present) was then subtracted. The intensity vs. q scattering patterns were normalized by their respective areas within the inspected q range and integrated across all points at the same q.

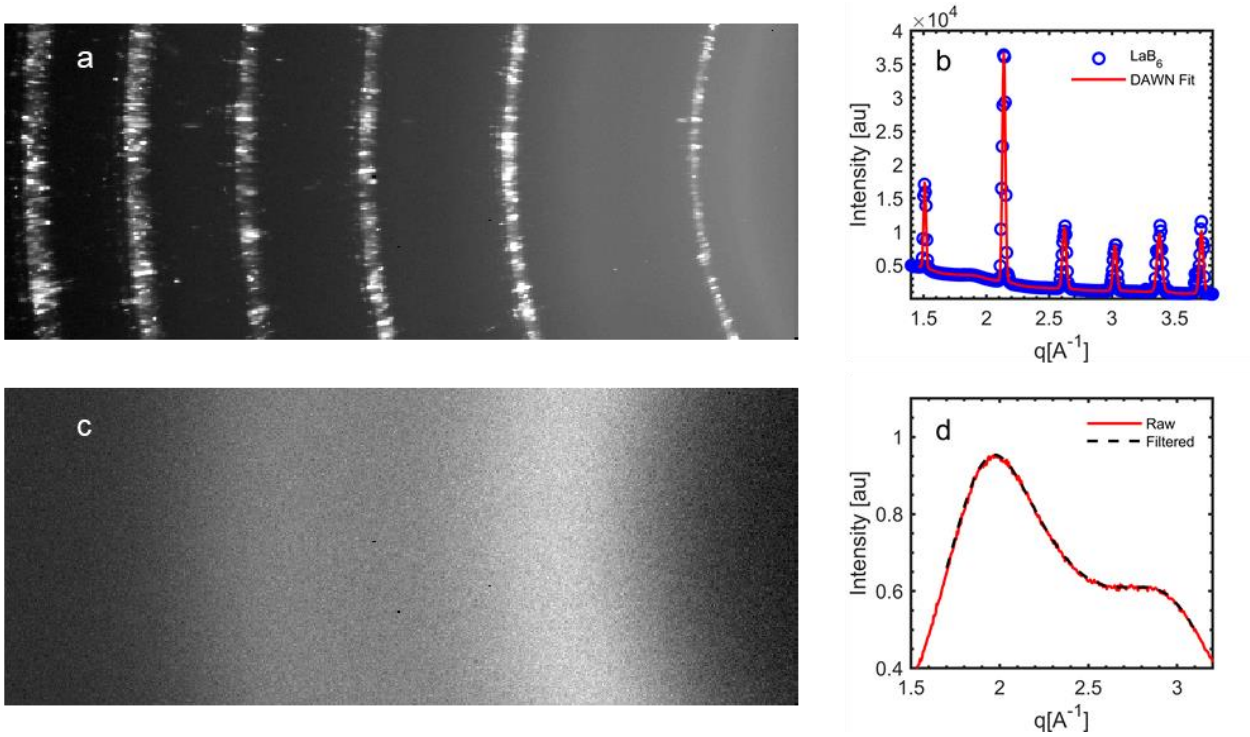

Fig. 2. (a) Powder diffraction image of LaB_6 for reference and (b) line plot after azimuthal integration. (c) Scattering intensity distribution of liquid water at 4 K,and (d) line plot after azimuthal integration in its raw form (after background subtraction) and filtered form.

Results and Discussion

Several characteristics of the scattering patterns vary with liquid temperature and were investigated as potential approaches for thermometry. These approaches include measurement of the intensity and location of the peak; higher order statistical moments of variance, skewness, and kurtosis of the patterns; and partial least squares (PLS) regression. Due to challenges with noise and measurement uncertainty, PLS was selected as the method for analysis. The scattering patterns and an appropriate statistical fit of water, ethanol, and *n*-dodecane are shown in Fig. 3.

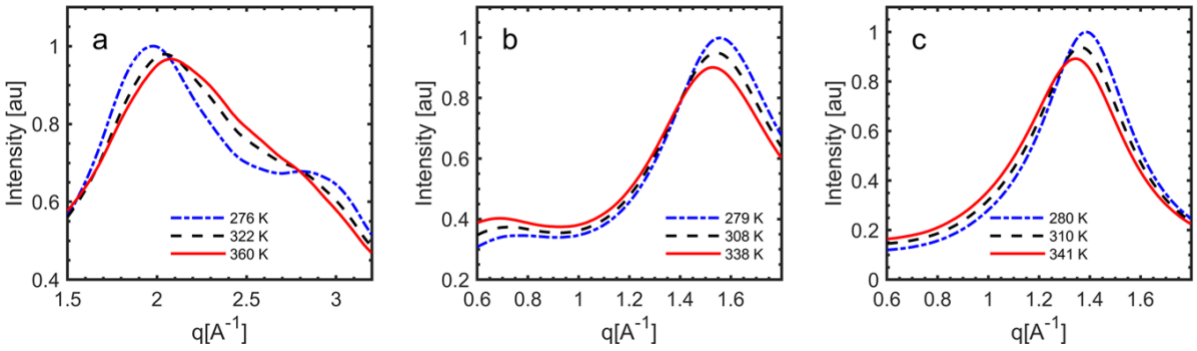

Fig. 3. Scattering patterns of (a) water, (b) ethanol, and (c) *n*-dodecane plotted in *q* space.

The scattering patterns in Fig. 3 show the change in scattering profile as a function of temperature. PLS regression on the scattering patterns was used to remove the collinearity and more easily construct a thermometer [37–38].

A PLS model was developed in Python using the PLS Regression module from the scikit-learn package [39] to extract the temperature from a given scattering profile. Training datasets of scattering profiles were individually collected for each of the liquids while the temperature was ramped up to higher levels. To remove experimental bias, the training datasets were standardized by centering the mean to zero and scaling by the standard deviation of the intensity values at each *q*. The PLS model was then constructed from the standardized training datasets, with the first few components explaining most of the variation with temperature.

A second visit to the APS was made to collect an independent set of X-ray scattering data to validate the results of the initial measurements. The data set was standardized in the same way as stated previously and converted to temperature using the same beta coefficient vector. Results of the temperature interpolation using the established PLS model is shown in Fig. 4. The calculated R^2 indicates the model captures 92% of the variation in the measured temperatures, whereas the

calculated root-mean-square error (RMSE) gives a prediction of ~6 K or less error for water, ethanol, and *n*-dodecane.

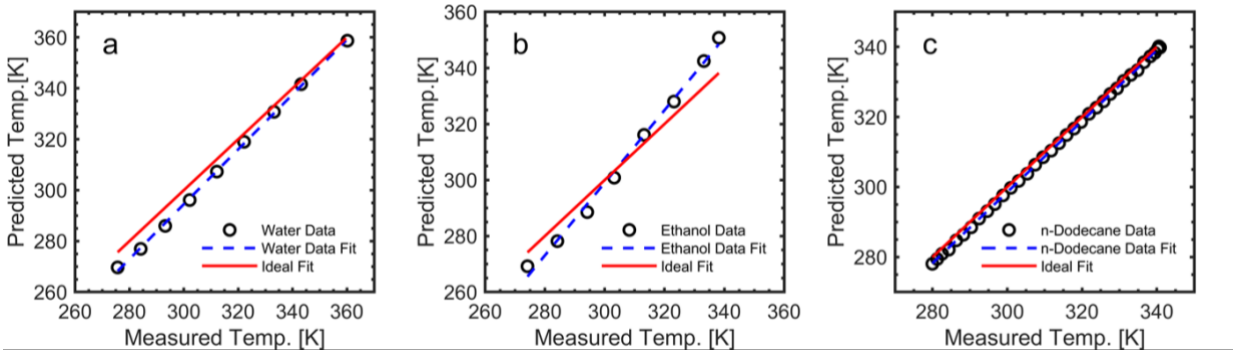

Fig. 4. Predicted temperatures (black symbols) of the (a) water, (b) ethanol, and (c) n-dodecane jets from scattering data collected during a second visit to APS using the PLS model constructed from the first trip, as compared with measured temperatures using an in-line thermocouple. The blue line is a linear fit to the predicted temperatures. The red line is the ideal scenario where the predicted and measured temperatures are equal.

This validation shows the repeatability of the method. Through application of PLS on the initial 487 data points in q space, only 2 components for water and ethanol and 3 components for *n*-dodecane were necessary to build the linear model. The use of additional components did not increase the accuracy of the measurements. The largest error of ~2% could be reduced with a more thorough calibration dataset for use in future measurements.

Conclusions

The feasibility of a novel X-ray diagnostic approach for tracer-free, liquid-phase temperature measurements in optically complex multiphase flows is described. The temperature sensitivity of X-ray scattering patterns in several liquids of interest for transportation and industrial processing applications was characterized. PLS regression was used to infer temperature from an unknown

scattering profile enabling measurements within ~2%. A potential drawback of a diagnostic technique relying on X-rays is that the method may be path integrated, which does not lend itself to planar imaging but may be extended to tomography. Future work includes exploring spatio-temporal features of sprays using point-wise raster scanning, investigating applicability in more dilute regions of the spray, collection of improved calibration data sets, testing and optimization in specific applications, and potential extension for use in liquid mixtures.

Funding

Benjamin Halls worked for the Air Force Research Laboratory (AFRL) when this data was collected. This manuscript has been cleared for public release by the AFRL (88ABW-2020-3228). A portion of this research was performed at the 7-BM beamline of the Advanced Photon Source, Argonne National Laboratory. Use of the APS is supported by the U. S. Department of Energy under Contract No. DE-AC02-06CH11357. This paper describes objective technical results and analysis. Any subjective views or opinions that might be expressed in the paper do not necessarily represent the views of the U.S. Department of Energy or the United States Government. Sandia National Laboratories is a multimission laboratory managed and operated by National Technology & Engineering Solutions of Sandia, LLC, a wholly owned subsidiary of Honeywell International Inc., for the U.S. Department of Energy's National Nuclear Security Administration under contract DE-NA0003525. SAND 2020-XXX

References

1. Epstein AH. "Aircraft engine's needs from combustion science and engineering. Combust Flame 2012; 159:1791–1792.
2. Lefebvre AH, McDonell VG. Atomization and Sprays, New York: Taylor and Francis; 1989.
3. Meyer TR, Brear M, Jin SH, Gord JR. Formation and Diagnostics of Sprays in Combustion. In: Handbook of Combustion. New York: Wiley; 2010.
4. Ashgriz N. Handbook of Atomization and Sprays. New York: Springer; 2011.

5. Lemoine F, Castanet G. Temperature and chemical composition of droplets by optical measurement techniques: a state-of-the-art review. Exp Fluids 2013; 54:1572.
6. Massoli P, Beretta F, D'Alessio A, Lazzaro M. Temperature and size of single transparent droplets by light scattering in the forward and rainbow regions. Appl Opt 1993; 32(18):3295–3301.
7. van Beeck JPAJ, Giannoulis D, Zimmer L, Riethmuller ML. Global rainbow thermometry for droplet-temperature measurement. Opt Lett 1999; 24(23):1696–1698.
8. Murray AM, Melton LA. Fluorescence methods for determination of temperature in fuel spray. Appl Opt 1985; 24(17):2783–2787.
9. Wells MR, Melton LA. Temperature Measurements of Falling Droplets. J Heat Trans 1990; 112(4):1008–1013.
10. Hanlon TR, Melton LA, Exciplex Fluorescence Thermometry of Falling Hexadecane Droplets. J Heat Trans 1992; 114(2):450–457.
11. Coppeta J, Rogers C. Dual emission laser induced fluorescence for direct planar scalar behavior measurements. Exp Fluids 1998; 25(1):1–15.
12. Lavieille P, Lemoine F, Lavergne G, Lebouché M. Evaporating and combusting droplet temperature measurements using two-color laser-induced fluorescence. Exp Fluids 2001; 31(1):45–55.
13. Maqua C, Castanet G, Lemoine F, Bicomponent droplets evaporation: Temperature measurements and modelling. Fuel 2008; 87(13–14):2932–2942.
14. Mishra YN, Nada FA, Polster S, Kristensson E, Berrocal E. Thermometry in aqueous solutions and sprays using two-color LIF and structured illumination. Opt Express 2016; 24(5):4949–4963.
15. Labergue A, Delconte A, Lemoine F. Study of the thermal mixing between two non-isothermal sprays using combined three-color LIF thermometry and phase Doppler analyzer. Exp Fluids 2013; 54:1527.
16. Hu H, Koochesfahani MM. A novel technique for quantitative temperature mapping in liquid by measuring the lifetime of laser induced phosphorescence. J Visualization 2003; 6(2):143–153.
17. Omrane A, Juhlin G, Ossler F, Aldén M. Temperature measurements of single droplets by use of laser-induced phosphorescence. Appl Opt 2004; 43(17):3523–3529.
18. Brübach J, Patt A, Dreizler A. Spray thermometry using thermographic phosphors. Appl Phy B 2006; 83:499.
19. Tropea C, Yarin AL, Foss JF. Temperature measurement via absorption, light scattering and laser-induced fluorescence. In: Experimental fluid mechanics. Berlin, 2007.
20. Wulsten E, Lee G. Surface temperature of acoustically levitated water microdroplets measured using infra-red thermography. Chem Eng Sci 2008; 63(22):5420–5424.
21. Akafuah NK, Salazar AJ, Saito K. Infrared thermography-based visualization of droplet transport in liquid sprays. Infrared Physics & Technology 2010; 53(3):218–226.
22. Saha A, Basu S, Kumar R. Particle image velocimetry and infrared thermography in a levitated droplet with nanosilica suspensions. Exp Fluids 2012; 52(3):795–807.
23. Talley DG, Thamban ATS, McDonell VG, Samuelsen GS. Laser sheet visualization of spray structure. In: Recent Advances in Spray Combustion: Spray Atomization and Drop Burning Phenomena. AIAA. 1995.
24. Sick V, Stojkovic B. Attenuation effects on imaging diagnostics of hollow-cone sprays. Appl Opt 2001; 40(15):2435–2442.
25. Linne MA. Imaging in the Optically Dense Regions of a Spray: A Review of Developing Techniques. Prog Energ Combust Sci 2013; 39(5):403–440.

26. Birk A, McQuaid M, Gross M. Liquid core structure of evaporating sprays at high pressures – Flash X-ray Studies. Report from the Army Research Lab. Aberdeen Proving Ground-TR-901 1995.
27. Halls BR, Heindel TJ, Meyer TR, Kastengren AL. Evaluation of X-ray sources for quantitative two- and three-dimensional imaging of liquid mass distribution in atomizing sprays. Int J Multiphas Flow 2014; 59:113–120.
28. Kastengren AL, Powell CF. Synchrotron X-ray techniques for fluid dynamics. Exp Fluids 2014; 55(3):1–15.
29. Halls BR, Radke CD, Reuter BJ, Kastengren AL, Gord JR, Meyer TR. High-Speed, Two-Dimensional Synchrotron White-Beam X-ray Radiography of Spray Breakup and Atomization. Opt Express 2017; 25(2):1605–1617.
30. Halls BR, Meyer TR, Kastengren AL. Quantitative Measurement of Binary Liquid Distributions Using Multiple-Tracer X-ray Fluorescence and Radiography. Opt Express 2015; 23(2):1730–1739.
31. Lin K-C, Rajnicek C, McCall J, Carter C, Fezzaa K. Investigation of pure- and aerated-liquid jets using ultra-fast X-ray phase contrast imaging. Nucl Instrum Meth A 2011; 649(1):194–496.
32. Lin K-C, Ryan M, Carter C, Sandy, A. Narayanan S, Ilavsky J, Wang J. Investigation of condensed supercritical ethylene jets using Small Angle X-ray Scattering (SAXS) technique. J Nucl Instrum Methods Phys Res A 2011; 649(1):219–221.
33. Sellberg JA, Huang C, McQueen TA, Loh ND, Laksmono H, Schlesinger D, et al. Ultrafast X-ray probing of water structure below the homogeneous ice nucleation temperature. Nature 2014; 510: 381–384.
34. Eng PJ, Newville M, Rivers ML, Sutton SR. Dynamically figured Kirkpatrick Baez x-ray micro-focusing optics. P Soc Photo-Opt Ins 1998; 3449:145–156.
35. Hubbell JH, Seltzer SM. 2004. Tables of X-Ray Mass Attenuation Coefficients and Mass Energy-Absorption Coefficients (version 1.4). [Retrieved 02, 20, 2013, from http://physics.nist.gov/xaamdi].
36. Filik, J, Ashton, AW, Chang, PCY, Chater, PA, Day, SJ, Drakopoulos, M, Gerring, MW, Hart, ML, Magdysyuk, OV, Michalik, S, Smith, A, Tang, CC, Terrill, NJ, Wharmby, MT, and Wilhelm, H, Processing two-dimensional X-ray diffraction and small-angle scattering data in DAWN 2, J. Appl. Crystallography 2017, 50(3), pp. 959–966.
37. Wold S, Sjöström M, Eriksson L. PLS-regression: a basic tool of chemometrics. Chemometrics and Intelligent Laboratory Systems 2001; 58:109–130.
38. Mevik B, Wehrens R. The pls Package: Principal Component and Partial Least Squares Regression in R. J Stat Softwar 2007, 18(2).
39. Scikit-learn: Machine Learning in Python, Pedregosa et al., JMLR 12, pp. 2825-2830, 201